Ocean Engineering 42 (2012) 155–164

Contents lists available at SciVerse ScienceDirect

Ocean Engineering

journal homepage: www.elsevier.com/locate/oceaneng

Simulation of large-amplitude motion of floating wind turbines using conservation of momentum

Lei Wang *,[1], Bert Sweetman

Texas A&M University, Department of Civil Engineering, College Station, TX 77843-3136, United States

ARTICLE INFO

Article history:
Received 17 May 2011
Accepted 3 December 2011
Editor-in-Chief: A.I. Incecik
Available online 28 January 2012

Keywords:
Floating wind turbines
Large-amplitude motion
Conservation of momentum
Simulation
Euler angles
Euler dynamic equations
Multi-body
Gyroscopic moments

ABSTRACT

A new method is presented to directly derive the nonlinear equations of motion (EOMs) of a floating wind turbine system using the theorem of conservation of angular momentum and Newton's second law. The methodology considers the system as two rigid bodies: the tower and the rotor-nacelle assembly (RNA). The large-amplitude rotation of the tower is described by the 1-2-3 sequence Euler angles, which offer accurate nonlinear coupling between motions in 6 degrees of freedom (DOFs). Two additional DOFs of the RNA relative to the tower, nacelle yaw and rotor spin, are prescribed by mechanical control and are also included in the EOMs of the entire system. Results from the EOMs are transformed among different coordinate systems at every time-step for use in the computation of hydrodynamics, aerodynamics and restoring forces, which preserves the nonlinearity between external excitation and structural dynamics. The new method is verified by critical comparison of simulation results with those of the popular wind turbine dynamics software FAST. The concept of highly compliant floating wind turbines is introduced. The large-amplitude motions and gyroscopic moments of one of these smaller, lighter structures is simulated in an example.

1. Introduction and background

Environmental, aesthetic and political pressures continue to push for siting offshore wind turbines beyond sight of land, where waters tend to be deeper, and use of floating structures is likely to be considered. Design of a floating wind turbine support structure capable of maintaining a near-vertical tower requires buoyancy far exceeding the weight of the equipment being supported. Savings could potentially be realized by reducing hull size, which would allow more compliance with the wind thrust force in the pitch direction. The loss of blade swept area has been shown to have a modest effect on energy capture (Wang and Sweetman, 2011). Increased dynamic motions does not necessarily correspond to increased dynamic load. For sinusoidal motion, the amplitude of the inertial loads is the product of the moment of inertia, amplitude of the motion and the square of the circular frequency. Decreasing the stiffness reduces the pitch and roll natural frequencies, which decreases inertial loading, but may require special consideration in the design of the rotor speed and blade-pitch controllers. Design of these increasingly compliant floating towers will make computation of structural dynamics both more challenging and more important, mainly because of the effects of gyroscopic moments. For conventional, stiff, bottom-founded structures, these moments are primarily generated by mechanical precession of the spin axis into the shifting winds, and so are limited by the maximum yaw rate (Henderson and Vugts, 2001). However, no such limit exists for gyroscopic moments of floating structures because they result from both shifting winds and irregular motions of the tower. New methodologies must be developed and employed to simulate the motions of new design concepts.

The compliant floating wind turbine system can be considered as a multi-body system including tower, rotor, nacelle and other moving parts, which are mechanically connected by the yaw bearing, hub, etc. One conventional analytical method to simulate the dynamics motions of such a system would be the Newton–Euler (NE) equations or Euler–Lagrange (EL) equations (Saha, 1999). The NE equations are usually established by separating the free-body diagrams of each rigid body in the system. For example, Stoneking (2007) presents the derivation of the exact nonlinear dynamic equations of motion for a multi-body spacecraft connected by spherical gimbal joints. Matsukuma et al. (Matsukuma and Utsunomiya, 2008) employ NE equations combined with constraint conditions associated with the joints between rigid bodies to analyze the dynamic response of a 2-MW downwind turbine mounted on a spar-type floating platform

Abbreviation: EOMs, equations of motion; DOFs, degrees of freedom; RNA, rotor-nacelle assembly.

* Corresponding author. Tel.: +1 409 740 4834; fax: +1 409 741 7153.
E-mail addresses: lei.ray@hotmail.com (L. Wang), sweetman@tamu.edu (B. Sweetman).
[1] Present address: Texas A&M University, Maritime Systems Engineering Department, 200 Seawolf Parkway, Galveston, TX 77553-1675, United States.

0029-8018/$ - see front matter © 2012 Elsevier Ltd. All rights reserved.
doi:10.1016/j.oceaneng.2011.12.004

for pitch amplitudes up to around 10° in steady wind, but no waves, and conclude that the platform motions are meaningfully influenced by gyro moments associated with rotor rotation. The EL equations apply energy methods to establish equations of motion for generalized degrees of freedom. Overall, the commonly used NE method computes the internal forcing between rigid bodies, and is excellent for applications in which the internal forcing has significant concern. However, for simulation of general motion of a system, these internal forces are not needed at every time step. The EL method is efficient for the solution of motion, while the derivation of partial derivatives of energy about related generalized DOFs is laborious. Additionally, the number of equations is equal to that of DOFs for previous conventional methods: the number of equations of the NE method is six times of number of rigid bodies within the multi-body system; the number of equations for the EL method is just that of the generalized DOFs. Kane's method combines the advantages of both the NE and EL methods. As the well-recognized wind turbine dynamics analysis software, the NREL FAST aero-elastic simulator (Jonkman and Buhl, 2005; Jonkman, 2007) uses Kane's method to derive the EOMs for the floating wind turbine system with rotations of platform less than 20°. In FAST, the hydrodynamic radiation-diffraction analysis package WAMIT (WAMIT 6.4, 2008) can be used to provide hydrodynamic forcing in the case of small-amplitude motions.

The work presented here is also a combination of the NE and EL methods for the computation of the general motion using only six equations no matter how many DOFs the system has. It makes direct use of the known interactions between mechanical components in the wind turbine, which are directly controlled or explicitly defined, to derive the rotational equations of motion of the entire wind turbine system. The conventional Euler dynamic equations are normally applied to only one rigid body, while the known relationships between the rigid body components enable the application of the theorem of conservation of angular momentum to the entire system. Transformation matrixes are used to transfer the angular momentum of each rigid body to a unified coordinate system to obtain the total angular momentum of the entire system, the derivative of which is equal to the sum of external moments applied to the system. The resulting rotational EOMs are combined with translational equations governed by Newton's second law of the entire multi-body system to develop a system of six equations. A key advantage of the new methodology is that the EOMs use fewer equations than previous conventional methods because only three rotational DOFs of the base body (tower) described by Euler angles and three translational DOFs need to be solved. Known relative DOFs along the rigid-body chain (nacelle yaw and blade spin) do not require additional EOMs. Structural flexibility of individual bodies cannot be considered using this method. However, neglecting these effects is reasonable for compliant design in cases where the global motions are dominated by first order rigid-body motions that are much larger than the higher modes allowed by structural flexibility. Mechanical systems with known geometric relationships between components are common, especially in rotating machinery. Thus, the methodology here is developed for floating wind turbine systems, but is broadly applicable to other types of interconnected dynamic mechanical systems.

The nonlinearities of various external forces and moments due to their coupling with structural motions are addressed in this work. Aerodynamics and hydrodynamics are calculated including the motion of body through the fluid, and the instantaneous position of the structure is accurately computed to incorporate nonlinearities of both the mooring and hydrostatics. In the numerical simulation, the motions and external excitation (including both external forces and moments) are transformed between various coordinate systems at each time step using matrices developed in terms of Euler angles for the rigid body. Thus, the full nonlinear coupling between external excitation and large-amplitude motion of the tower is preserved.

2. Coordinate systems and Euler angles

The methodology considers the system as two rigid bodies: the tower is the complete structural assembly, including the buoyant hull, that supports the rotor-nacelle assembly (RNA); the RNA is the complete assembly that can mechanically yaw relative to the tower. The implementation of the new method requires use of several coordinate systems to derive the EOMs for the complete system. The external excitation applied in the dynamic equations is computed consecutively and projected into the corresponding coordinate systems. Fig. 1 shows both the (X,Y,Z) and the (X_M,Y_M,Z_M) systems, which are earth-fixed global coordinate systems with the origin located at the center of mass (CM) of the entire system and still water level respectively in case of equilibrium status of the system with zero displacements. The (x_t,y_t,z_t) and the (A,B,C) systems are body fixed and originate at the CM of the tower and RNA, respectively. The CM of the RNA, G_R, is assumed to be on the centerline of the tower to guarantee that the CM of the system, G_s, is fixed on the tower. The (x_s,y_s,z_s) system is parallel to (x_t,y_t,z_t) and originates at the instantaneous CM of the entire system, which is also assumed to be on the centerline of the tower. Thus (x_s,y_s,z_s) coincides with the (X,Y,Z) system for zero displacement.

The (X,Y,Z) and (x_s,y_s,z_s) coordinate systems are used for application of both the Newton's second law and the theorem of moment of momentum on the entire system. Two body-fixed

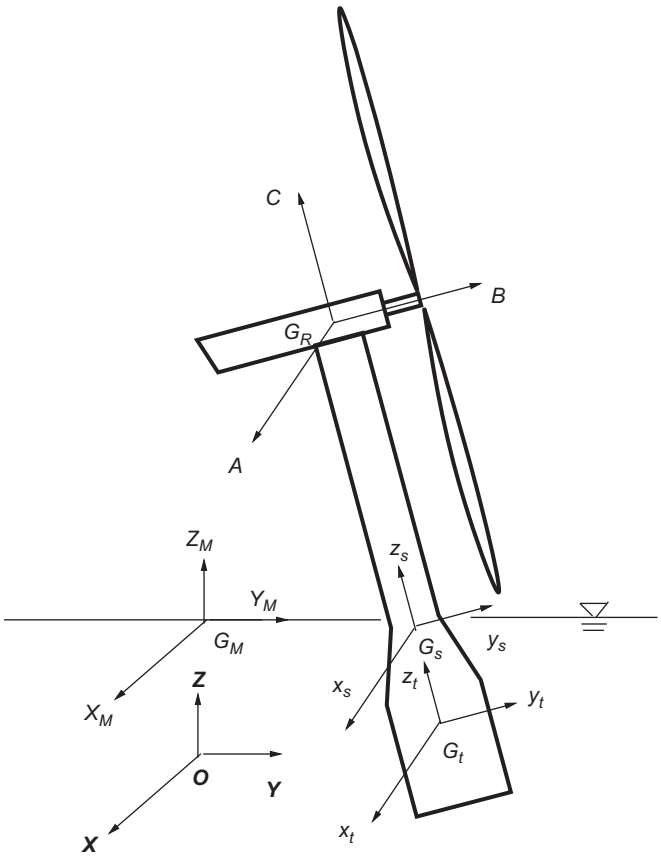

Fig. 1. Coordinate systems used in the application.

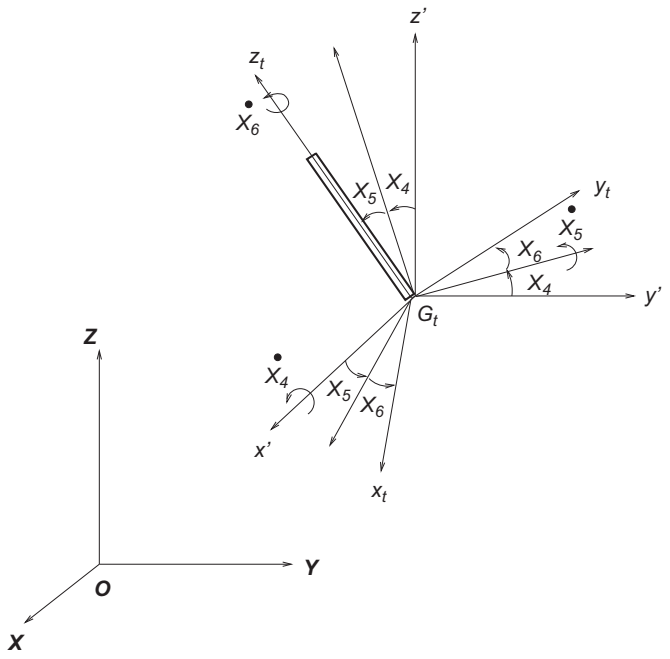

Fig. 2. 1-2-3 sequenced Euler angles in terms of X_4, X_5 and X_6.

Cartesian frames, (A,B,C) and (x_t,y_t,z_t), are assumed to be on the principal axes of inertia in order to simplify the calculation of angular momentum of the two rigid bodies. The (A,B,C) system is assumed to be on the principal axes of both the rotor and the nacelle. The (X_M,Y_M,Z_M) system is defined to enable comparison of simulation results with those of FAST, in which the reference point is usually prescribed to be on the still water level.

Fig. 2 shows the Euler angles used to describe large-amplitude rotational motion. For large angular displacements in space, the order in which the angles of rotation are applied is important; there are 12 possible Euler angles sequences. Here, 1-2-3 sequenced Euler angles X_4–X_5–X_6 are used to describe the position of the rotating tower. The (x',y',z') is translating coordinate system with respect to the (X,Y,Z) system, with the origin located at the CM of the tower. The (x_t,y_t,z_t) system can be transformed from the (x',y',z') by: first rotating the upright tower about the x'-axis by angle X_4, and then rotating about the resulting second coordinate axis through an angle X_5, and finally, rotating the tower about the z_t-axis through the third Euler angle, X_6.

3. Equation of motion of the system

The well-known Euler equations of motion are conventionally derived using conservation of angular momentum applied to a single rigid body. Here, the theorem of moment of momentum is directly applied to the complete wind turbine system, which consists of two rigid bodies: the tower and the RNA. Six unknown DOFs of tower (translation and rotation) and two known DOFs of RNA (nacelle yaw and rotor spinning) are considered in the model. Using the presented method, only one set of equations of motion are needed to compute the rotational dynamics of the integrated multi-body system. The angular momentum of the entire system results from the sum of angular momentum of each rigid body, which is computed within the respective local coordinate system and then transformed into a unified system with the origin located on the CM of the wind turbine system. Similar to the application of Newton–Euler dynamics equations to one rigid body, the coupled motions are computed using rotational EOMs combined with translational equations governed by Newton's Second Law of multi-body systems.

Beginning with conservation of angular momentum, the sum of the moments resulting from externally applied forces about the CM of a system of particles in the translating-rotating system, (x_s,y_s,z_s), equals the change of amplitude of the momentum within the coordinate system plus the change of direction of the momentum with respect to global coordinate system (e.g. Hibbeler, 2004)

$$\sum \vec{M} = \vec{H}^{\dot{s}}_{G_s} = (\vec{H}^{\dot{s}}_{G_s})_{x_s y_s z_s} + \vec{\omega}_t \times \vec{H}^{s}_{G_s} \tag{1}$$

The L.H.S. of Eq. (1), $\sum \vec{M}$, represents the moments from all of external forces: $\sum \vec{M} = \vec{M}_{wind} + \vec{M}_{wave} + \vec{M}_{restoring}$, where the restoring moment $\vec{M}_{restoring}$ includes the effect of both hydrostatics and mooring lines; the environmental moments $\vec{M}_{wind}$ and $\vec{M}_{wave}$ result from wind and wave forces. In the R.H.S. of Eq. (1), $\vec{H}^{s}_{G_s}$ is the angular momentum of entire system calculated about that CM of the multi-body system and decomposed into the (x_s,y_s,z_s) system. The vector $\vec{\omega}_t$ describes the angular velocity of (x_s,y_s,z_s) with respect to the global coordinate system (X,Y,Z), which is the absolute angular velocity of the tower because the (x_s,y_s,z_s) system is parallel to the body-fixed coordinate system (x_t,y_t,z_t). In general, angular momentum of a system, $\vec{H}^{s}_{G_s}$, can be decomposed into any coordinate system with the origin located at the CM of the entire multi-body system. Here, choosing the orientation of (x_s,y_s,z_s) parallel to (x_t,y_t,z_t) simplifies the calculation of angular momentum and its derivative. The angular momentum of the system, $\vec{H}^{s}_{G_s}$, is obtained by superimposing the momenta of the RNA and the tower and then decomposing the sum onto the (x_s,y_s,z_s) system: $\vec{H}^{s}_{G_s} = \vec{H}^{R}_{G_s} + \vec{H}^{t}_{G_s}$, in which the angular momenta of two rigid bodies, $\vec{H}^{R}_{G_s}$ and $\vec{H}^{t}_{G_s}$, are calculated about the CM of the system, G_s. These momenta can be further related to the angular momenta about the respective CM of these two rigid bodies by (e.g. Hibbeler, 2004)

$$\vec{H}^{t}_{G_s} = \vec{\rho}_{G_t/G_s} \times m_t \vec{v}_{G_t} + \vec{H}^{t}_{G_t} \tag{2}$$

$$\vec{H}^{R}_{G_s} = \vec{\rho}_{G_R/G_s} \times m_R \vec{v}_{G_R} + \vec{H}^{R}_{G_R} \tag{3}$$

where radius vectors, $\vec{\rho}_{G_R/G_s}$ and $\vec{\rho}_{G_t/G_s}$, are from G_s to the CM of RNA and tower, respectively, and projected onto the (x_s,y_s,z_s) system; $\vec{v}_{G_R}$ and $\vec{v}_{G_t}$ represent the corresponding linear velocities of the CM; m_R and m_t are the masses of these two rigid bodies. Those terms including radius vectors correspond to the effect of distance in the parallel axis theorem, and can be further represented by expanding $\vec{v}_{G_R}$ and $\vec{v}_{G_t}$ in terms of the linear velocity of G_s, $\vec{v}_{G_s}$

$$\vec{\rho}_{G_t/G_s} \times m_t \vec{v}_{G_t} = \vec{\rho}_{G_t/G_s} \times m_t (\vec{v}_{G_s} + \vec{\omega}_t \times \vec{\rho}_{G_t/G_s}) \tag{4}$$

$$\vec{\rho}_{G_R/G_s} \times m_R \vec{v}_{G_R} = \vec{\rho}_{G_R/G_s} \times m_R (\vec{v}_{G_s} + \vec{\omega}_t \times \vec{\rho}_{G_R/G_s}) \tag{5}$$

Combining Eqs. (4) and (5)

$$\begin{aligned}\vec{\rho}_{G_t/G_s} \times m_t \vec{v}_{G_t} + \vec{\rho}_{G_R/G_s} \times m_R \vec{v}_{G_R} = {} & \vec{\rho}_{G_t/G_s} \times (m_t \vec{\omega}_t \times \vec{\rho}_{G_t/G_s}) \\ & + \vec{\rho}_{G_R/G_s} \times (m_R \vec{\omega}_t \times \vec{\rho}_{G_R/G_s})\end{aligned} \tag{6}$$

Those terms including the linear velocity of the CM of the system disappear because $m_R \vec{\rho}_{G_R/G_s} + m_t \vec{\rho}_{G_t/G_s} = 0$, which decouples the angular momentum of the system and its derivative from the translational DOFs. This decoupling significantly simplifies solution of Eq. (1), which increases the efficiency of numerical solution to the final coupled 6-DOFs equations of motion.

The angular momentum of the tower, $\vec{H}^{t}_{G_t}$ in Eq. (2), is calculated in the (x_t,y_t,z_t) coordinate system, parallel to the (x_s,y_s,z_s) system, and originated from the CM of the tower. If the body-fixed coordinate system (x_t,y_t,z_t) are composed of principal axes of inertia, the angular momentum of the tower can be obtained by first calculating the product of the inertia tensors and the angular velocities, and then transforming into the (x_s,y_s,z_s) system: $\vec{H}^{t}_{G_t} = T_{t\to s}(I_t \vec{\omega}_t)$, where $T_{t\to s}$ is the transformation matrix from (x_t,y_t,z_t) to (x_s,y_s,z_s) and equal to

the elementary matrix because these two coordinate systems are parallel; the inertia tensor of the tower, I_t, is a diagonal matrix with diagonal elements equal to I_{x_t}, I_{y_t} and I_{z_t}, i.e. the moments of inertia of the tower about its principal axes. The absolute angular velocity of the tower, $\vec{\omega}_t$, is decomposed into the body fixed coordinate system (x_t,y_t,z_t) and can be represented in terms of 1-2-3 sequenced Euler angles by (e.g. Zeng and Shen, 2005)

$$\vec{\omega}_t = \begin{bmatrix} \dot{X}_4 \cos X_5 \cos X_6 + \dot{X}_5 \sin X_6 \\ -\dot{X}_4 \cos X_5 \sin X_6 + \dot{X}_5 \cos X_6 \\ \dot{X}_4 \sin X_5 + \dot{X}_6 \end{bmatrix} \tag{7}$$

The angular momentum of the RNA in Eq. (3), $\vec{H}^R_{G_R}$, is calculated by further separating the RNA into the nacelle and the rotor (including all spinning parts within the RNA). The (A,B,C) system is assumed to be the principal coordinate system of inertia of the nacelle. The angular momentum of the nacelle is transformed from its principal axes to the (x_s,y_s,z_s) by: $\vec{H}^n_{G_R} = T_{n\to s}(I_n\vec{\omega}_n)$, in which $T_{n\to s}$ is the transformation matrix from (A,B,C) to (x_s,y_s,z_s); I_n is the inertia tensor of the nacelle calculated about the (A,B,C) system. The angular velocity of the nacelle within the (A,B,C) system, $\vec{\omega}_n$, is obtained by first calculating it in the (x_t,y_t,z_t) system in terms of nacelle yaw rate and then transforming into the (A,B,C) system: $\vec{\omega}_n = T_{t\to n}\vec{\omega}_{n,t} = T_{t\to n}(\vec{\omega}_t + \vec{\omega}_{yaw})$, where the transformation matrix from (x_t,y_t,z_t) to (A,B,C), $T_{t\to n}$, can be calculated by the inverse of $T_{n\to s}$, which is just the transpose since the transformation matrix is orthogonal; $\vec{\omega}_{n,t}$ represents the absolute angular velocity of the nacelle with respect to the (x_t,y_t,z_t) system; the vector $\vec{\omega}_{yaw}$ has positive nacelle yaw rate component along z_t-direction, i.e. $\vec{\omega}_{yaw}=(0,0,\omega_{yaw})$.

Here, the (A,B,C) axes are assumed to be on the principal axes of the rotor to simplify the calculation of angular momentum. This angular momentum depends on both the moments of inertia and the angular velocities of the rotor in the (A,B,C) system. The exact moments of inertia of the rotor are preserved in the (A,B,C) system and are not the function of time. Similar to the calculation of $\vec{\omega}_n$, the angular momentum of the rotor can be calculated by: $\vec{H}^r_{G_R} = T_{n\to s}I_r\vec{\omega}_{r,n} = T_{n\to s}I_r(\vec{\omega}_n + \dot{\vec{\psi}})$, in which $\vec{\omega}_{r,n}$ represents the absolute angular velocity of the rotor with respect to the (A,B,C) system; I_r is the inertia tensor of the rotor calculated about the (A,B,C) system; the spinning vector $\dot{\vec{\psi}}$ has a positive component about B-direction, i.e. $\dot{\vec{\psi}} = (0,\dot{\psi},0)$. Combining the angular momentums of nacelle and rotor, the angular momentum of RNA is $\vec{H}^n_{G_R} + \vec{H}^r_{G_R} = T_{n\to s}(I_n+I_r)\vec{\omega}_n + T_{n\to s}I_r\dot{\vec{\psi}}$, in which the moments of inertia of the nacelle and rotor can be combined into that of RNA within the (A,B,C) system

$$\vec{H}^R_{G_R} = T_{R\to s}(I_R\vec{\omega}_n) + T_{R\to s}I_R\dot{\vec{\psi}} \tag{8}$$

In Eq. (8), the nacelle and the rotor are treated as a single unit, with yaw motion along the C-axis and spinning motion along the B-axis. The change of I_r to I_R directly has no influence on the calculation because in the inertia tensor, only that element associated with spinning matters in this term. Considering the (A,B,C) system as the principal coordinate system of inertia of the RNA, the transformation matrix from (A,B,C) to (x_s,y_s,z_s), $T_{R\to s}$, is equal to $T_{n\to s}$ and can be represented as Eberly (2008)

$$T_{R\to s}(\beta) = \begin{bmatrix} \cos\beta & -\sin\beta & 0 \\ \sin\beta & \cos\beta & 0 \\ 0 & 0 & 1 \end{bmatrix} \tag{9}$$

where the relative degree of freedom, β, describes the rotation of (A,B,C) to (x_s,y_s,z_s) and depends on the yaw angle of the nacelle, which is continually adjusted by the yaw control mechanism; I_R is the inertia tensor of the RNA in the form of diagonal matrix with diagonal elements equal to I_A, I_B and I_C. Combining Eqs. (2) and (3), the angular momentum of the system in the (x_s,y_s,z_s) system, $\vec{H}^s_{G_s}$, can be arranged as: $\vec{H}^s_{G_s} = I_s\vec{\omega}_t + \vec{H}'$, which is a generalized validation of Leimanis's conclusion (Leimanis, 1965): the angular momentum of a two-rigid-body system can be separated into one part due to transport of the whole system considered as a rigid body and another part due to the relative motion between the bodies. The inertia tensor associated with the transport of the system, I_s, can be expressed as

$$I_s = \begin{bmatrix} I_{11} & I_{12} & I_{13} \\ I_{21} & I_{22} & I_{23} \\ I_{31} & I_{32} & I_{33} \end{bmatrix} \tag{10}$$

in which

$$I_{11} = (I_A\cos^2\beta + I_B\sin^2\beta + m_R\rho^2_{G_R/G_s}) + (I_{x_t} + m_t\rho^2_{G_t/G_s})$$

$$I_{12} = (I_A - I_B)\cos\beta\sin\beta$$

$$I_{21} = (I_A - I_B)\cos\beta\sin\beta$$

$$I_{22} = (I_A\sin^2\beta + I_B\cos^2\beta + m_R\rho^2_{G_R/G_s}) + (I_{y_t} + m_t\rho^2_{G_t/G_s})$$

$$I_{33} = I_C + I_{z_t}$$

$$I_{13} = I_{23} = I_{31} = I_{32} = 0$$

where ρ_{G_t/G_s} and ρ_{G_R/G_s} are the moduli of corresponding vectors in Eqs. (2) and (3). The off-diagonal terms in the inertia tensor result from the included angle between the B and y_s-axes. The effect of the parallel axis theorem is obvious in the diagonal terms. The angular momentum of the RNA relative to the tower can be expressed by collecting terms independent of the rotation of the tower, $\vec{\omega}_t$: $\vec{H}' = (-I_B\dot{\psi}\sin\beta, I_B\dot{\psi}\cos\beta, I_C\omega_{yaw})$. The angular momentum associated with the spinning blades corresponds to projections onto both x_s- and y_s-directions, while the angular momentum associated with the nacelle yaw is only along the z_s-axis.

The absolute time derivative in Eq. (1) includes changes in both the direction and amplitude of the angular momentum vector. The latter can be expressed as

$$(\dot{\vec{H}}^s_{G_s})_{x_sy_sz_s} = \dot{I}_s\vec{\omega}_t + I_s\dot{\vec{\omega}}_t + \dot{\vec{H}}' \tag{11}$$

where the derivative of inertia tensor, $\dot{I}_s$, is computed by taking time derivative element by element in the matrix according to the definition of matrix derivative. Thus, only the time-dependent terms in the inertia tensor are considered, which include the angle β since $\dot{\beta} = \omega_{yaw}$. This derivative of angular momentum is simplified considerably by the selection of the (x_s,y_s,z_s) system parallel to the body fixed (x_t,y_t,z_t), because all the time-dependent terms are explicitly defined by the yaw control mechanism and the geometrical configuration.

Computation of transitional motions is relatively straightforward. The theorem of the motion of the center of mass is applied to the entire wind turbine system to solve the translational DOFs

$$\sum\vec{F} = m_s\vec{a}_{G_s} \tag{12}$$

where $\vec{a}_{G_s}$ is the linear acceleration of the CM of the system, $\vec{a}_{G_s} = (\ddot{X}_1,\ddot{X}_2,\ddot{X}_3)$; m_s is the mass of the whole system; the force vector $\sum\vec{F}$ represents the external forces of the entire system in the inertia coordinate system (X,Y,Z), including environmental forces, restoring forces and gravity: $\sum\vec{F} = \vec{F}_{wind} + \vec{F}_{wave} + \vec{F}_{restoring} + \vec{G}$. Each of these components must be decomposed to the inertia coordinate system (X,Y,Z) for application of Newton's second law. Restoring forces, $\vec{F}_{restoring}$, include contributions from buoyancy of the hull and tension of the mooring lines.

4. Restoring forces

The restoring forces (including both the external forces and moments) resulting from the contribution of hydrostatics and mooring lines are also computed for large-amplitude motions. Restoring forces are calculated about the CM of the system, G_s, which may experience large excursions from the original equilibrium position. The large-amplitude motions preclude use of the conventional stiffness matrix method in which restoring forces can be computed as a stiffness matrix times a displacement vector with each column of the matrix corresponding to unit motion in one DOF and zero displacements in other DOFs. This section addresses the nonlinear hydrostatic and mooring forcing due to coupled large-amplitude translational and rotational motions.

The LHS of the rotational equations of motion (Eq. (1)) is the sum of the external moments in the translating-rotating system (x_s,y_s,z_s); the LHS of the translational equations (Eq. (12)) is the external forces in the inertial system (X,Y,Z). The transformation matrix between these two coordinate systems is a function of 1-2-3 sequenced Euler angles X_4–X_5–X_6 since the (x_s,y_s,z_s) system is defined parallel to the body-fixed coordinate system of the tower, (x_t,y_t,z_t). The transformation matrix from (x_s,y_s,z_s) to (X,Y,Z) can be expressed as

$$T_{s\to I}=T_x(X_4)T_y(X_5)T_z(X_6)=\begin{bmatrix} t_{11} & t_{12} & t_{13}\\ t_{21} & t_{22} & t_{23}\\ t_{31} & t_{32} & t_{33}\end{bmatrix} \tag{13}$$

in which

$$t_{11}=\cos X_5\cos X_6$$

$$t_{12}=-\cos X_5\sin X_6$$

$$t_{13}=\sin X_5$$

$$t_{21}=\cos X_4\sin X_6+\cos X_6\sin X_4\sin X_5$$

$$t_{22}=\cos X_4\cos X_6-\sin X_4\sin X_5\sin X_6$$

$$t_{23}=-\cos X_5\sin X_4$$

$$t_{31}=\sin X_4\sin X_6-\cos X_4\cos X_6\sin X_5$$

$$t_{32}=\cos X_6\sin X_4+\cos X_4\sin X_5\sin X_6$$

$$t_{33}=\cos X_4\cos X_5$$

where $T_x(X_4)$, $T_y(X_5)$ and $T_z(X_6)$ are element transformation matrices (Sweetman and Wang, 2011). The complexity of Eq. (13) results from prescribing the (x_s,y_s,z_s) system parallel to the (x_t,y_t,z_t) system instead of the (X,Y,Z) system. This resulting complexity is more than offset by avoiding the tedious calculation of the time derivative of this transformation matrix.

The hydrostatic restoring forces are calculated directly from the buoyancy of the cylindrical floater. The instantaneous buoyancy of a floating cylinder in the inertial coordinate system (X,Y,Z) is $\vec{F}_B^I=(0,0,\rho g\pi r^2h_1)$ (Zeng and Shen, 2005), where ρ is the density of sea water; g is the gravitational acceleration; r is the radius of the cylinder; h_1 is instantaneous submerged length of the cylinder along the centerline. This variable length is a function of heave motion and leaning angle of the cylinder

$$h_1=\frac{\rho_{G_M/O}-X_3}{\cos\theta_1}-\rho_{G_M/O}+h_0 \tag{14}$$

where $\rho_{G_M/O}$ is the distance measured from still water level to the CM of the system in its equilibrium position, i.e. the length from G_M to O in Fig. 1; θ_1 is the leaning angle of the cylinder with respect to vertical, $\cos\theta_1=\cos X_4\cos X_5$; h_0 is the initial length of h_1, i.e. the draft of cylinder in equilibrium position. For small rotations, the restoring force in heave reduces to the conventional $F_B=\rho g\pi r^2(h_0-X_3)$.

The center of buoyancy of a partially submerged cylinder piercing the water surface at an angle is described by the radius vector in the (x_s,y_s,z_s) system, i.e. $\vec{\rho}_{B/G_s}=(x_s^B,y_s^B,z_s^B)$, in which (Zeng and Shen, 2005)

$$x_s^B=-\frac{t_{31}r^2}{4t_{33}h_1}$$

$$y_s^B=-\frac{t_{32}r^2}{4t_{33}h_1}$$

$$z_s^B=\vec{h}_G+\frac{h_1}{2}+\frac{r^2(t_{31}^2+t_{32}^2)}{8t_{33}^2h_1} \tag{15}$$

where vector $\vec{h}_G$ indicates the position of the bottom of the cylinder measured from the (x_s,y_s,z_s) system along the centerline. To obtain the hydrostatic restoring moment in the (x_s,y_s,z_s) system, the buoyancy in the inertia coordinate system is decomposed into the (x_s,y_s,z_s) system and then combined with the vector radius $\vec{\rho}_{B/G_s}$, i.e. $\vec{F}_B^s=T_{I\to s}\vec{F}_B^I$ and $\vec{M}_B^s=\vec{\rho}_{B/G_s}\times\vec{F}_B^s$, in which the transformation matrix from (X,Y,Z) to (x_s,y_s,z_s), $T_{I\to s}$, is the inverse of Eq. (13), which is just the transpose since the transformation matrix is orthonormal. This hydrostatic calculation method is applicable to any composite body having a cylinder piercing the water-plane. The center of buoyancy of fully submerged parts of a composite body are not affected by pitch angle, and can be geometrically combined with a surface-piercing cylinder.

A simplified mooring system is assumed to consist of four radial taut lines for convenience. The change in tension in each line can easily be expressed as a function or cable stretch. Each fairlead position is calculated by summing translations and Euler angle rotations. The contribution of each mooring line is calculated consecutively and then summed. The combined restoring force in the (X,Y,Z) system and the combined restoring moment calculated about G_s in the (x_s,y_s,z_s) system are needed in the application of equations of motion of the system.

Compliance along each straight line is due to elasticity of the materials only. The radius position of any one fairlead (point A) in the inertia coordinate system (X,Y,Z) is $\vec{\rho}_{A/O}=\vec{\rho}_{G_s/O}+T_{s\to I}\vec{\rho}_{A/G_s}$, where the radius vector $\vec{\rho}_{G_s/O}$ is the position of G_s measured from the (X,Y,Z) system, $\vec{\rho}_{G_s/O}=(X_1,X_2,X_3)$ and $\vec{\rho}_{A/G_s}$ is the radius position of point A in the (x_s,y_s,z_s) system. The position of the fixed end (point E) of this mooring line on the sea bottom, $\vec{\rho}_{E/O}$, is constant in the (X,Y,Z) system. Combining, the radius position from point A to point E in the (X,Y,Z) system is $\vec{\rho}_{E/A}=\vec{\rho}_{E/O}-\vec{\rho}_{A/O}$. The tension along a neutrally buoyant taut line in the (X,Y,Z) system can be obtained by the nature of elasticity material (Zeng and Shen, 2005)

$$\vec{F}_{line}^I=\left[T_0+\frac{ES}{L}(\rho_{E/A}-L)\right]\frac{\vec{\rho}_{E/A}}{\rho_{E/A}} \tag{16}$$

where T_0 is the pretension of one mooring line; E is Young's Modulus; S is the cross sectional area of the line; L is the initial length of the line; $\rho_{E/A}$ is the norm of the vector $\vec{\rho}_{E/A}$, i.e. the instantaneous length of the line. The restoring force of the mooring system, $\vec{F}_{mooring}^I$, is obtained by summing the force from each line.

The restoring moment from each line in the (x_s,y_s,z_s) system is obtained by decomposing the restoring force into the (x_s,y_s,z_s) system first and then multiplied by the radius vector of the fairlead, i.e. $\vec{F}_{line}^s=T_{I\to s}\vec{F}_{line}^I$ and $\vec{M}_{line}^s=\vec{\rho}_{A/G_s}\times\vec{F}_{line}^s$. The result from each line can be further summed to obtain the restoring moment from mooring system, $\vec{M}_{mooring}^s$. Finally, the restoring

forces can be expressed as

$$\vec{F}_{restoring} = \vec{F}^{I}_{B} + \vec{F}^{I}_{mooring} \tag{17}$$

$$\vec{M}_{restoring} = \vec{M}^{S}_{B} + \vec{M}^{S}_{mooring} \tag{18}$$

5. Environmental forcing

The wind force in the (X,Y,Z) system and wind moment calculated about G_s in the (x_s,y_s,z_s) system are needed in the application of equations of motion of the system. For simplicity, an approximate wind thrust force is computed for the complete swept area of the blades following the method of Nielsen et al. (2006):

$$F_b = \tfrac{1}{2} C_T \rho_a A_b V_{rb}^2 \tag{19}$$

where ρ_a is the density of air; A_b is the swept area of the blades; C_T is the thrust coefficient; V_{rb} is the amplitude of the velocity of the wind relative to the RNA along the B-axis. The wind force is assumed to be applied on the center of the blade area and along the B-axis, i.e., perpendicular to the blade area. The thrust coefficient, C_T, is assumed to depend solely on relative wind velocity and is taken directly from Nielsen (Nielsen et al., 2006) and repeated in Fig. 3. This curve is a proxy for the influence of conventional blade-pitch control on thrust. The curve was developed by assuming that the control mechanism maximizes the power output for wind speeds below the rated speed (8.7 m/s here) and retains constant power output after the rated speed. More accurate wind forces could be computed by linking the codes of this method with an existing rotor-aerodynamics module, e.g. AeroDyn (Laino and Hansen, 2011).

The amplitude of relative velocity, V_{rb}, is computed by projecting both the wind velocity and structural velocity onto the B-axis. A unit vector $\vec{u}^{I}_{B}$ indicates the direction of the B-axis in the (X,Y,Z) system by $\vec{u}^{I}_{B} = T_{R\to I}\vec{u}^{R}_{B}$, where $\vec{u}^{R}_{B}$ is the unit vector along B-axis in the (A,B,C) system, i.e. $\vec{u}^{R}_{B} = (0,1,0)$. The transformation matrix from (A,B,C) to (X,Y,Z), $T_{R\to I}$, is obtained by multiplication of the transformation matrix in Eqs. (9) and (13): $T_{R\to I} = T_{s\to I}T_{R\to s}$.

The structural velocity of the center of the blade area can be expressed as: $\vec{V}^{I}_{G_R} = \vec{V}_{G_s} + T_{s\to I}(\vec{\omega}_t \times \vec{\rho}_{G_R/G_s})$, where $\vec{V}_{G_s}$ is the linear velocity of G_s in the inertial coordinate system (X,Y,Z): $\vec{V}_{G_s} = (\dot{X}_1,\dot{X}_2,\dot{X}_3)$ and the distance between G_R and the center of the hub is neglected. Projections of the wind velocity and structural velocity along the B-axis are obtained by dot product:

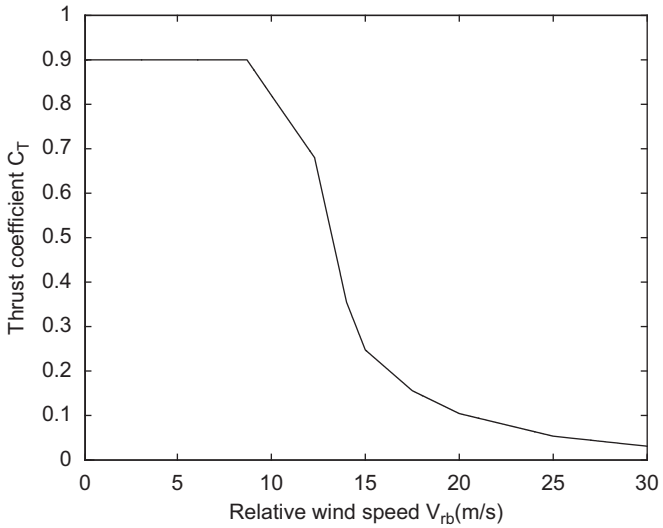

Fig. 3. Thrust force coefficient as a function of relative wind velocity (Nielsen et al., 2006).

$V_w = \vec{V}^{I}_{wind}\cdot\vec{u}^{I}_{B}$ and $V_b = \vec{V}^{I}_{G_R}\cdot\vec{u}^{I}_{B}$, in which $\vec{V}^{I}_{wind}$ is the wind velocity in the (X,Y,Z) system. The amplitude of relative velocity in Eq. (19) is obtained by $V_{rb} = V_w - V_b$. Finally the wind force in the (X,Y,Z) system and the wind moment in the (x_s,y_s,z_s) system are expressed as

$$\vec{F}_{wind} = T_{R\to I}\vec{F}^{R}_{wind} \tag{20}$$

$$\vec{M}_{wind} = \vec{\rho}_{G_R/G_s} \times \vec{F}^{R}_{wind} \tag{21}$$

where $\vec{F}^{R}_{wind}$ is the wind force in the (A,B,C) system: $\vec{F}^{R}_{wind} = (0,-F_b,0)$. The aerodynamic torque is modeled as a constant using rated power divided by rotor speed, which is added to the wind moment.

Similar to the calculation of restoring forces, wave forces are computed in the (X,Y,Z) coordinate system and then decomposed into the (x_s,y_s,z_s) system to compute the moments. The generalized Morison equation is used to calculate the wave forces per unit length normal to the axis of the leaning cylinder (e.g., Sarpkaya and Issacson, 1981)

$$\vec{f}^{I}_{n} = C_m\rho\frac{\pi}{4}D^2\dot{\vec{V}}_n - C_a\rho\frac{\pi}{4}D^2\dot{\vec{V}}_t + \frac{1}{2}\rho C_d D\vec{V}_{rt}|\vec{V}_{rt}| \tag{22}$$

where ρ is the density of sea water; D is the local diameter of the hull; C_m is the inertia coefficient; C_a is the added mass coefficient, and C_d is the drag coefficient. All velocities and accelerations are normal to the central axis of the tower: $\dot{\vec{V}}_n$ is the normal component of wave acceleration; $\dot{\vec{V}}_t$ is the normal component of structural acceleration; $\vec{V}_{rt}$ is the normal velocity of the water particle relative to the cylinder. The term associated with C_a in Eq. (22) is usually considered as the added mass. Hydrodynamic damping is included considering the relative velocity in the drag force calculation. Use of the Morison equation implicitly assumes the body has a negligible effect on the incident waves, which is reasonable here because the hull structure is relatively slender. Also, as is conventional for use of the Morison equations, dynamic pressures along the axis of the cylinder are neglected.

A unit vector along the central axis of the tower is needed to define the normal direction of kinematic vectors, i.e. $\vec{e}^{I}_{3} = T_{s\to I}\vec{e}^{t}_{3}$, where $\vec{e}^{t}_{3}$ is a unit vector along centerline of the tower in the (x_t,y_t,z_t) system, i.e. $\vec{e}^{t}_{3} = (0,0,1)$, and is transformed to the (X,Y,Z) system. Thus, the normal component of water particle acceleration can be expressed as: $\dot{\vec{V}}_n = \vec{e}^{I}_{3}\times(\dot{\vec{V}}\times\vec{e}^{I}_{3})$, where $\dot{\vec{V}}$ is the wave acceleration vector in the (X,Y,Z) system. The structural velocity and acceleration of the segment along the tower can be obtained by the kinematics of rigid body

$$\vec{V}_t = \vec{V}_{G_s} + T_{s\to I}(\vec{\omega}_t \times \vec{\rho}_{i/G_s}) \tag{23}$$

$$\dot{\vec{V}}_t = \vec{a}_{G_s} + T_{s\to I}[\dot{\vec{\omega}}_t \times \vec{\rho}_{i/G_s} + \vec{\omega}_t \times (\vec{\omega}_t \times \vec{\rho}_{i/G_s})] \tag{24}$$

where $\vec{V}_{G_s}$ and $\vec{a}_{G_s}$ are the linear velocity and acceleration of the CM of the system, G_s, in the inertial coordinate system (X,Y,Z); $\vec{\rho}_{i/G_s}$ is the vector radius from G_s to the segment with unit length. The wave kinematic velocity relative to the moving tower, $\vec{V}_{rt}$, is expressed as: $\vec{V}_{rt} = \vec{e}^{I}_{3}\times(\vec{V}_r\times\vec{e}^{I}_{3})$, where $\vec{V}_r$ is the relative velocity of the wave to the segment of the submerged tower: $\vec{V}_r = \vec{V} - \vec{V}_t$, in which $\vec{V}$ is the wave kinematic velocity in the (X,Y,Z) system. The wave force on the cylinder, $\vec{F}_{wave}$, is obtained by summing the force on each segment from Eq. (22). The wave moment in the (x_s,y_s,z_s) coordinate system can be computed by transforming the resulting forces from Eq. (22) into the (x_s,y_s,z_s) system and then

numerically integrating over the submerged length of the tower

$$\vec{F}_{wave} = \int_r \vec{f}_n^I \, dr \tag{25}$$

$$\vec{M}_{wave} = \int_r (\vec{\rho}_{i/G_s} \times \vec{f}_n^s) \, dr \tag{26}$$

where $\vec{f}_n^s = T_{I\to s}\vec{f}_n^I$.

6. RNA moments and gyroscopic moments

Computation of the RNA moments and gyroscopic moments is not necessary to simulate the global motions of the tower. However, these internal moments between RNA and tower, especially gyro moments, are a significant concern in design, and can be calculated by application of the Euler dynamic equations about the rigid body RNA

$$\sum \vec{M}_R = \vec{H}_{G_R}^{\dot{R}} = (\vec{H}_{G_R}^{\dot{R}})_{ABC} + \vec{\omega}_n \times \vec{H}_{G_R}^R \tag{27}$$

where the angular momentum of the RNA is decomposed to the (A,B,C) system with angular velocity $\vec{\omega}_n = (\omega_{n,A},\omega_{n,B},\omega_{n,C})$ and can be represented as $\vec{H}_{G_R}^R = [I_A\omega_{n,A}, I_B(\omega_{n,B}+\dot{\psi}), I_C\omega_{n,C}]$. The reaction moments of $\sum \vec{M}_R$ are defined as RNA moments applied by RNA on the top of tower $(MRNA_A, MRNA_B, MRNA_C)$. The gyro moments are that part of the RNA moments resulting from the time derivative of angular momentum associated with the spinning rate in Eq. (27). If the (A,B,C) system is used to decompose the angular momentum of the gyro, the absolute time derivative is $\dot{\vec{H}}_{G_R}^{gyro} = (\dot{\vec{H}}_{G_R}^{gyro})_{ABC} + \vec{\omega}_n \times \vec{H}_{G_R}^{gyro}$, where the angular momentum related to spin can be expressed in the (A,B,C) system as $\vec{H}_{G_R}^{gyro} = (0, I_B\dot{\psi}, 0)$. Thus, the time change of the amplitude of this angular momentum within the (A,B,C) system, $(\dot{\vec{H}}_{G_R}^{gyro})_{ABC}$, is zero for constant spinning rate. Further, the gyro moments applied by the RNA on the top of the tower are

$$M_{G_R}^{gyro} = -\vec{\omega}_n \times \vec{H}_{G_R}^{gyro} = \begin{bmatrix} I_B\dot{\psi}\omega_{n,C} \\ 0 \\ -I_B\dot{\psi}\omega_{n,A} \end{bmatrix} \tag{28}$$

The gyro moments have non-zero components in the A- and C-directions, both of which are perpendicular to the spin vector along the B-axis. The cross product in the equations of motion results in the transfer of angular momenta between the A- and C-directions. The angular velocity of the nacelle of a rigid bottom-fixed wind turbine is always along the C-axis and equal to the yaw rate, ω_{yaw}. In this case, the gyro moments can be reduced to $(I_B\dot{\psi}\omega_{yaw}, 0, 0)$, which is the conventional expression for gyro moment in nutation (Henderson and Cheng, 2002). The angular velocity of the nacelle for a floating wind turbine also has a non-zero component in the A-direction, which results in a component of gyro moments in the C-direction and proportional to the angular velocity of the nacelle along the A-axis (Eq. (28)).

7. Example

Two different support-structure designs are used to demonstrate the new method. First, the OC3-Hywind model (Jonkman, 2010) is used to verify the new method presented here by comparison with the popular wind turbine dynamics software FAST (Jonkman, 2007) for a small-amplitude motion case. The OC3 Hywind is a conceptual design of the Hywind system developed to support the NREL 5-MW wind turbine. This design is stiff in pitch rotation and provides a realistic benchmark case against industry-standard software. The mooring system of OC3 Hywind is simplified by using two linear springs with stiffness equal to 5×10^4 N/m in the surge and sway directions such that it could be modeled in both FAST and the new method for verification. A truncated cylinder model is developed on the basis of OC3 Hywind. The new model has the subsurface buoyant cylinder truncated to reduce the available hydrostatic restoring moment, effectively allowing larger pitch angles. This second model demonstrates the new method for large-amplitude motion. The RNA for each model is based on that of OC3 Hywind: the moments of inertia of the RNA about the (A,B,C) coordinate system are $I_A = 2.35\times10^7$ kg m^2, $I_B = 4.37\times10^7$ kg m^2, $I_C = 2.54\times10^7$ kg m^2; the rotor speed is 12.1 rpm. The submerged length of the truncated model is reduced from the 120 m of OC3 Hywind to 72 m. The tower between the hull and RNA is based on OC3 Hywind and treated as a rigid body and its moments of inertia are combined with those of the hull: 3.57×10^9 kg m^2 and 9.28×10^7 kg m^2 in the tilt (roll and/or pitch) and yaw, respectively. The four taught-leg mooring lines are each assumed to be a straight axial spring with stiffness of 3.37×10^5 N/m and length of 295-m in a 320-m water depth location.

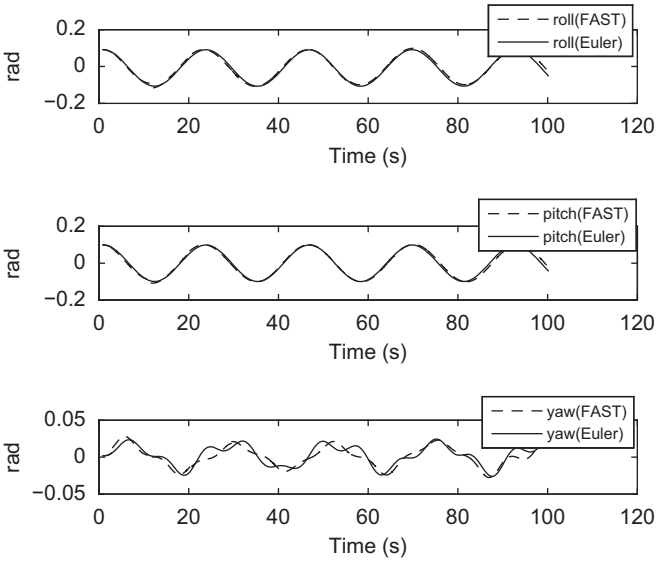

Fig. 4. Rotation comparison.

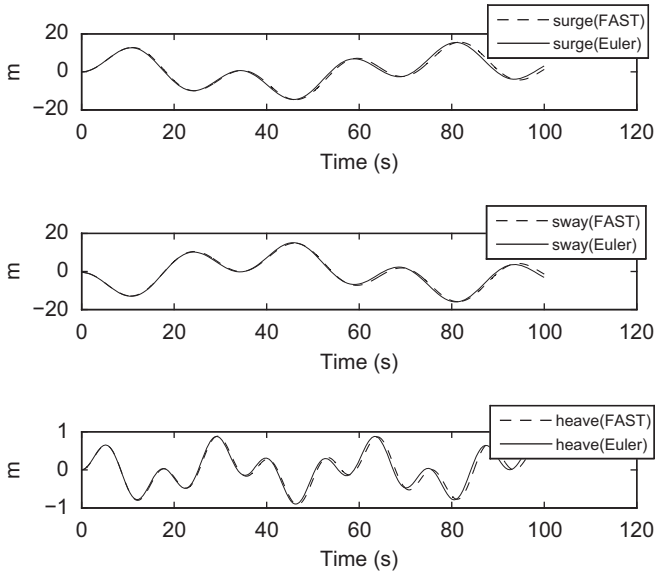

Fig. 5. Translation comparison.

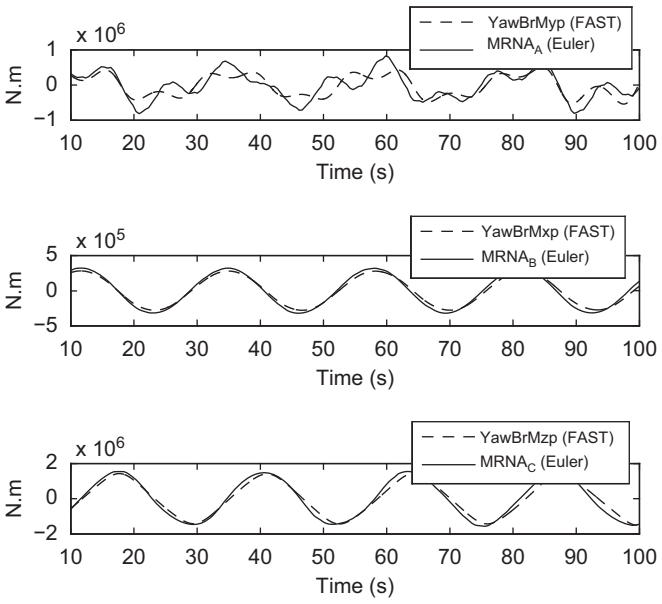

Fig. 6. RNA moments comparison.

7.1. Free vibration verified by FAST

Figs. 4–6 show the comparison of time histories from FAST and the method presented here for a small-amplitude free vibration case including blade spin but no nacelle yaw. Here both hydrodynamics and aerodynamics have been turned off in FAST. The only external forces acting on the body are from the mooring lines and buoyancy, both of which are represented simply in the user-defined subroutine (UserPtfmLd) as a 6×6 restoring matrix, in FAST. Stiffness values are linearized to be consistent with the method presented in Section 4 and tuned to reproduce the correct natural frequencies. The initial conditions of FAST are prescribed as roll equal to 0.1 rad, pitch equal to 0.1 rad and sway equal to 0.5 m with respect to a reference point on still water level. The Euler rotations are roughly equivalent to roll, pitch and yaw in FAST for small-amplitude rotation (Abkowitz, 1969). Rotational results in FAST are defined about the inertial reference frame and superimposed. The small-amplitude assumption leads to a nearly orthogonal transformation matrix, which is corrected by Frobenius Norm to guarantee its orthogonality (Jonkman, 2007), while the new method does not need any correction in terms of the superposition of rotational motion. It can be seen in Figs. 4–6 that both the motions and moments from the new method match the results of FAST very well. One inconsistency between the models is that FAST considers relative motion within the RNA while the new method considers a unified RNA with a single spin rate. In Fig. 4, the yaw motion results from excitation by the gyro moments along the centerline of the tower. The translation shown in Fig. 5 is measured from the reference point on still water level, the origin of (X_M,Y_M,Z_M) system. In Fig. 6, the RNA moments are compared to the internal moments in the tower-top coordinate system located at the yaw bearing in FAST, which is similar to the (A,B,C) coordinate system in absence of nacelle yaw, located at the center of the RNA. Figs. 4–6 show good agreement for this small-amplitude case and agreement improves for decreasing amplitudes. The next two example cases are for large-amplitude motion of the truncated spar model.

7.2. Forced vibration without nacelle yaw

Figs. 7–9 show results for the more compliant truncated spar model in a large-amplitude forced-vibration case. Environmental

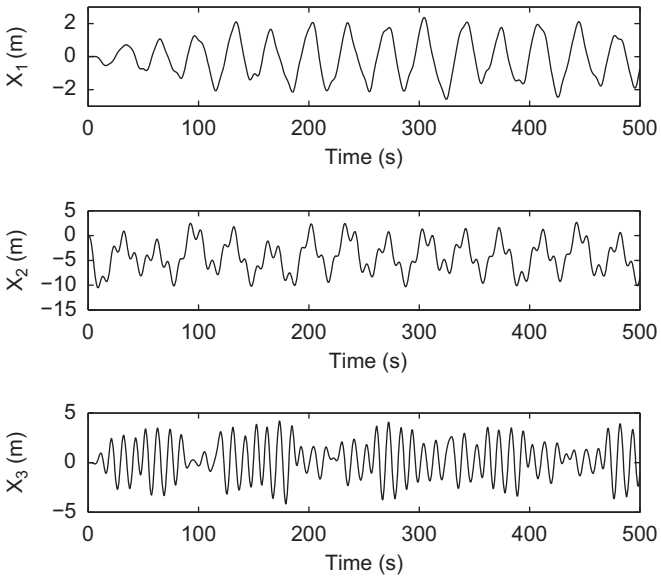

Fig. 7. Translational motion without nacelle yaw.

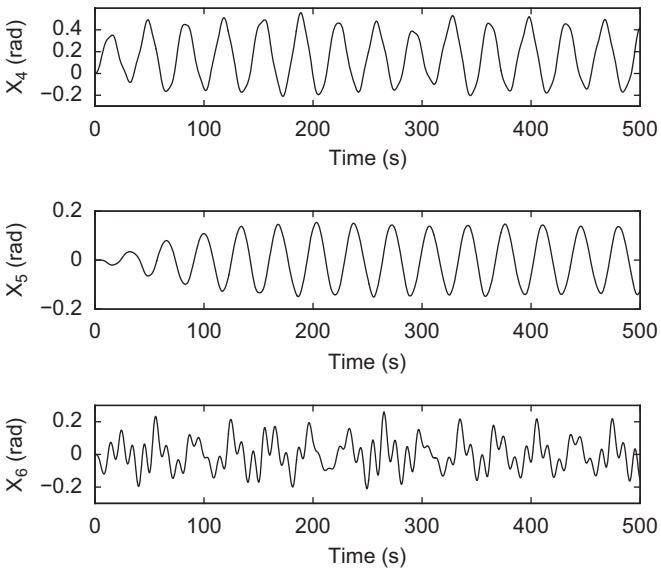

Fig. 8. Rotational motion without nacelle yaw.

loading is computed using irregular winds and waves along the negative direction of the Y-axis. The mean wind velocity at hub height is 18.2 m/s. Irregular wind velocities are simulated using TurbSim (Kelley and Jonkman, 2008). The wave environment is represented by a JONSWAP spectrum with a significant wave height of 5.0 m and peak period of 10 s. Wave forces are computed using the Morison equation from a first-order time-domain representation of irregular waves simulated directly from the wave spectrum using a uniform phase distribution. The inertia coefficient C_m in Eq. (22) is assumed to be 2.0; the added mass coefficient C_a is assumed to be 1.0; the drag coefficient C_d is assumed to be 0.6. Figs. 7–9 show the 6-DOFs motions of the tower and gyro moments without consideration of nacelle yaw, i.e. without relative motion between the nacelle and the tower. In Fig. 7, the translation of the tower is measured from the CM of the entire wind turbine system, i.e. the origin of (X,Y,Z) system in Fig. 1. The nonzero mean of X_2 results from the surge motion in the wind direction. Fig. 8 shows 1-2-3 sequenced Euler angles X_4, X_5 and X_6, which describe the large-amplitude rotational motion of the tower. The gyro moments shown in Fig. 9

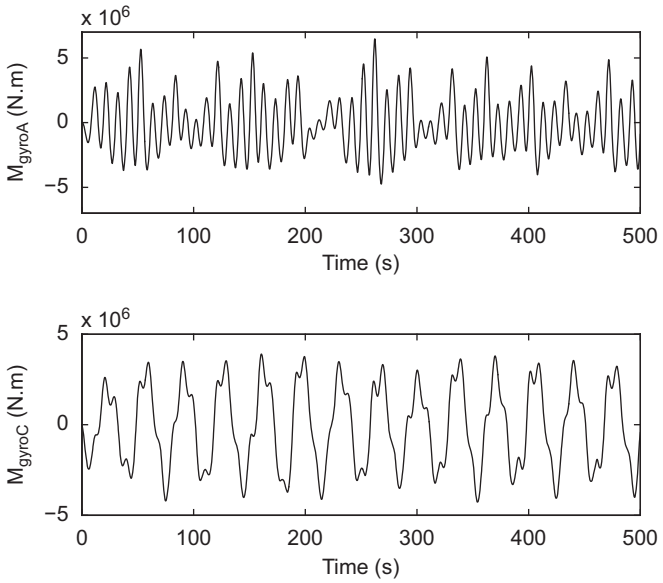

Fig. 9. Gyro moments without nacelle yaw.

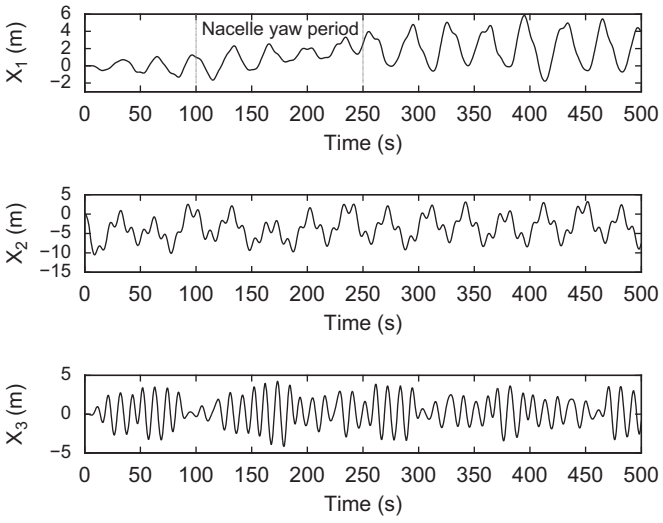

Fig. 10. Translational motion with nacelle yaw.

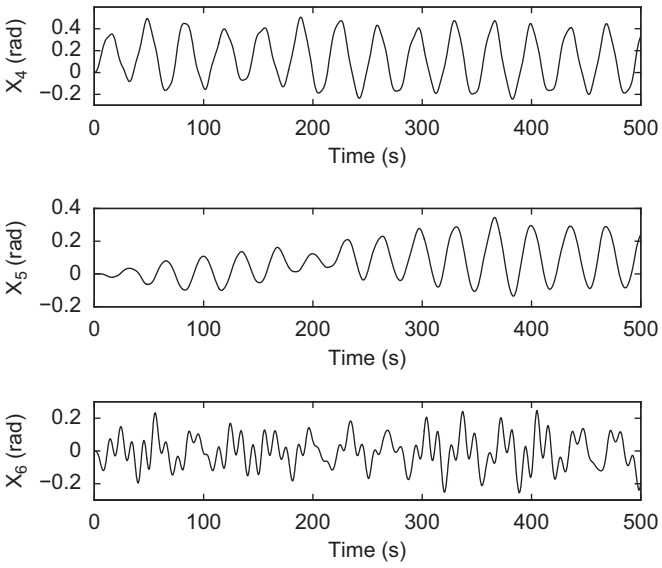

Fig. 11. Rotational motion with nacelle yaw.

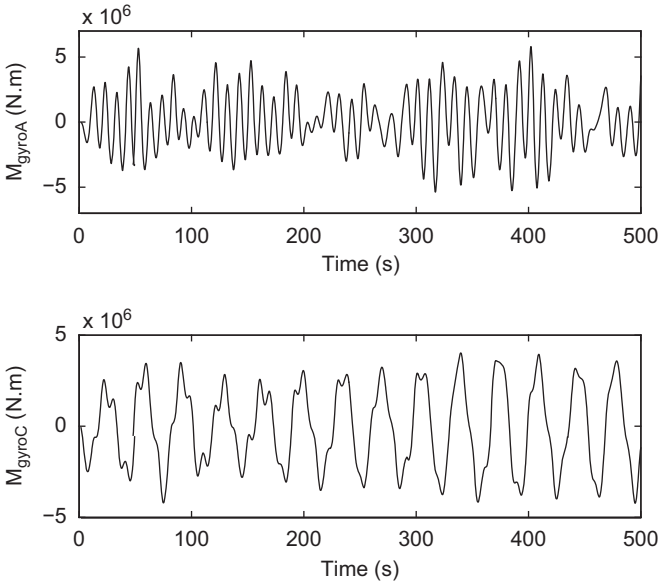

Fig. 12. Gyro moments with nacelle yaw.

are significant and cannot be ignored in the design. Different from the bottom-fixed wind turbine, the gyro moment in the *A*-direction still exists due to the self-rotation of tower about its centerline even in the absence of nacelle yaw. The gyro moment in the *C*-direction results from the angular velocity of tilt motion, and has the same frequency as X_4. Thus, the frequency of gyro moment is relevant to the frequency of motion of the tower and further depends on the frequency of environmental forcing.

7.3. Forced vibration with nacelle yaw

Figs. 10–12 show results for the same compliant spar model and the same wave conditions as the previous case, but with a sudden wind-shift imposed to show the effect of nacelle yaw. The wind direction is along the negative direction of the *Y*-axis during the first 100 s and then rotates by $\pi/4$ rad toward the negative direction of the *X*-axis in the *XOY* plane to simulate the sudden shift. The yaw rate of the nacelle is 0.3°/s. The wind shift causes the yaw control mechanism of the nacelle to activate at 100 s and deactivate at around 250 s. Fig. 10 shows the translation of the tower measured from the CM of the entire system. The amplitude of X_1-direction motion increases because the new wind direction results in a larger wind force in the sway direction. Similarly, the Euler angle X_5 increases as shown in Fig. 11 after the wind direction changes. Comparison of Figs. 12 and 9 indicates the nacelle yaw does not significantly change the amplitudes of the gyro moments. These yaw-induced moments are relatively small because the yaw rate is much smaller than the angular velocity of self-rotation of the tower about its centerline.

8. Conclusions

A new method has been developed to directly apply Newton's second law of the system and the theorem of conservation of angular momentum to an entire floating wind turbine system including RNA and tower, resulting in a new formulation to simulate translation and large-amplitude rotation of the system. Motions of an 8-DOFs system are represented as six EOMs of the tower. The 1-2-3 sequence Euler angles are introduced to describe

the rotation of the tower and the transformation matrixes between various coordinate systems. The restoring forcing and environmental forcing are calculated by considering nonlinear coupling among translational and rotational DOFs. Further, motions and external forcing are transformed at each time step between different coordinate systems. The fully nonlinear coupling between external forcing and large-amplitude motion of the system is also preserved. The new method is verified by comparison with the well-known software FAST for a small-amplitude case, for which the nonlinear coupling effects are small. Simulation results in terms of 6-DOFs motions of tower and gyro moments for the floating wind turbine with large-amplitude motions are also shown. A major strength of this new method is that it can be readily expanded to a large number of rigid bodies as long as the relative motion between contiguous bodies is explicitly defined. The decoupling of translational and rotational accelerations also dramatically increases the efficiency of numerical integration.

Acknowledgments

This work was supported by the National Science Foundation, Division of Civil and Mechanical Systems under Agreement Number CMS-0448730 and by the Division of Power, Controls and Adaptive Networks, agreement number PCAN-1133682. Any opinions, findings, and conclusions or recommendations expressed in this material are those of the authors and do not necessarily reflect the view of the National Science Foundation.

References

Abkowitz, M.A., 1969. Stability and Motion Control of Ocean Vehicles. MIT Press.
Eberly, D., 2008. Euler angle formulas. Technical Report. Geometric Tools, LLC. ⟨http://www.geometrictools.com/⟩.
Henderson, A.R., Cheng, P.W., 2002. Wave loads and slender offshore structures, comparison of theory & measurement. In: Proceedings of the Sixth German Wind Energy Conference "Where industry meets science".
Henderson, A.R., Vugts, J.H., 2001. Prospects for floating offshore wind energy. In: Proceedings of the European Wind Energy Conference.
Hibbeler, R.C., 2004. Engineering Mechanics—Statics and Dynamics. Pearson, Prentice-Hall.
Jonkman, J., 2010. Definition of the Floating System for Phase IV of OC3. Technical Report NREL/TP-500-47535. NREL National Energy Renewal Laboratory.
Jonkman, J.M., 2007. Dynamic Modeling and Loads Analysis of an Offshore Floating Wind Turbine. Technical Report NREL/TP-500-41958. NREL National Energy Renewal Laboratory.
Jonkman, J.M., Buhl, M.L.J., 2005. FAST User's Guide. Technical Report NREL/EL-500-38230. National Renewable Energy Laboratory.
Kelley, N., Jonkman, B., 2008. NWTC Design Codes (Turbsim). Technical Report. National Renewable Energy Lab. ⟨http://wind.nrel.gov/designcodes/⟩.
Laino, D.J., Hansen, A.C., 2011. User's Guide to the Wind Turbine Aerodynamics Computer Software AeroDyn. Technical Report. NREL National Energy Renewal Laboratory. ⟨http://wind.nrel.gov/designcodes/simulators/aerodyn/⟩.
Leimanis, E., 1965. The General Problem of the Motion of Coupled Rigid Bodies About a Fixed Point. In: Springer Tracts in Natural Philosophy.
Matsukuma, H., Utsunomiya, T., 2008. Motion analysis of a floating offshore wind turbine considering rotor-rotation. IES J. Part A: Civil. Struct. Eng. 1, 268–279.
Nielsen, F.G., Hanson, T.D., Skaare, B., 2006. Integrated dynamic analysis of floating offshore wind turbines. In: Proceedings of the International Conference on Offshore Mechanics and Arctic Engineering.
Saha, S., 1999. Dynamics of serial multibody systems using the decoupled natural orthogonal complement matrices. J. Appl. Mech. 66, 986–996.
Sarpkaya, T., Issacson, M., 1981. Mechanics of Wave Forces on Offshore Structures. Van Nostrand Reinhold Company.
Stoneking, E., 2007. Newton-euler dynamic equations of motion for a multi-body spacecraft. In: AIAA Guidance, Navigation, and Control Conference, pp. 1368–1380.
Sweetman, B., Wang, L., 2011. Large-angle rigid body dynamics of a floating offshore wind turbine using euler's equations of motion, in: NSF CMMI Research and Innovation Conference: Engineering for Sustainability and Prosperity.
WAMIT 6.4, 2008. WAMIT: The State of the Art in Wave Interaction Analysis—User Manual. Department of Ocean Engineering, MIT.
Wang, L., Sweetman, B., 2011. Conceptual design of floating wind turbines with large-amplitude motion, in: Proceedings of Society of Naval Architects and Marine Engineers.
Zeng, X.H., Shen, X.P., 2005. Nonlinear dynamics response of floating circular cylinder with taut tether. In: Proceedings of Fifteenth Offshore and Polar Engineering Conference, pp. 218–224.